




RESEARCH ARTICLE | AUGUST 09 2023

Metal–dielectric optical microcavity with tunable Q factor

G. A. Romanenko ; P. S. Pankin  ; D. S. Buzin ; D. N. Maksimov ; V. S. Sutormin ;
A. I. Krasnov ; F. V. Zelenov ; A. N. Masyugin ; S. V. Nedelin ; N. A. Zolotovskiy ; I. A. Tambasov ;
M. N. Volochaev ; K.-P. Chen ; I. V. Timofeev 

 Check for updates

Appl. Phys. Lett. 123, 061113 (2023)
<https://doi.org/10.1063/5.0157430>


View
Online


Export
Citation

CrossMark

Articles You May Be Interested In

Experimental implementation of tunable hybrid Tamm-microcavity modes

Appl. Phys. Lett. (October 2021)

The ITEP study of inclusive pion double charge exchange: Experiment and interpretation

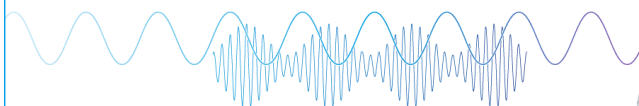
AIP Conference Proceedings (December 2001)

Morphological and electro optic studies of polymer dispersed liquid crystal in reverse mode

AIP Conference Proceedings (May 2018)

Webinar

Boost Your Signal-to-Noise Ratio with Lock-in Detection



Sep. 7th – Register now

 Zurich
Instruments

Metal–dielectric optical microcavity with tunable Q factor

Cite as: Appl. Phys. Lett. **123**, 061113 (2023); doi: [10.1063/5.0157430](https://doi.org/10.1063/5.0157430)

Submitted: 8 May 2023 · Accepted: 27 July 2023 ·

Published Online: 9 August 2023



View Online



Export Citation



CrossMark

G. A. Romanenko,^{1,2,3} P. S. Pankin,^{2,4,a)} D. S. Buzin,^{2,4} D. N. Maksimov,^{2,4} V. S. Sutormin,^{2,4} A. I. Krasnov,^{2,4} F. V. Zelenov,^{3,5} A. N. Masyugin,^{3,5} S. V. Nedelin,^{4,6} N. A. Zolotovskiy,^{4,6} I. A. Tambasov,^{2,4,6} M. N. Volochaev,² K.-P. Chen,⁷ and I. V. Timofeev^{2,4}

AFFILIATIONS

¹Krasnoyarsk Scientific Center, Siberian Branch, Russian Academy of Sciences, Krasnoyarsk 660036, Russia

²Kirensky Institute of Physics, Federal Research Center KSC SB RAS, Krasnoyarsk 660036, Russia

³Siberian State University of Science and Technology, Krasnoyarsk 660037, Russia

⁴Siberian Federal University, Krasnoyarsk 660041, Russia

⁵AO NPP Radiosvyaz, Krasnoyarsk 660021, Russia

⁶LLC Research and Production Company “Spectehnauka,” Krasnoyarsk 660043, Russia

⁷Institute of Photonics Technologies, National Tsing Hua University, Hsinchu 30013, Taiwan

^{a)} Author to whom correspondence should be addressed: pavel-s-pankin@iph.krasn.ru

ABSTRACT

We consider a layered metal–dielectric microcavity with a liquid crystal used as a resonator layer. The transformation of the microcavity spectra is shown experimentally using three methods, namely, mechanical rotation of the sample, heating, and applying external voltage. The obtained spectra exhibit multiple vanishing resonant lines. It is found the vanishing resonant lines are not a spectral manifestation of the bound state in the continuum for this system. Despite the absence of true bound states in the continuum, an experimental tuning of the resonance Q factor via changing the radiation loss rate is demonstrated through variation of the optical properties of the liquid crystal layer.

Published under an exclusive license by AIP Publishing. <https://doi.org/10.1063/5.0157430>

The bound state in the continuum (BIC) is a nonradiative localized state of an open system.¹ The existence of the BIC was theoretically predicted in Ref. 2–5 for the eigenvalue problem for a quantum particle with an energy above the oscillating and exponentially decaying potential. The simplest type symmetry-protected BICs (SP-BICs) are implemented in a system with the orthogonal localized and propagating modes.⁶ In 1985, Friedrich and Wintgen first demonstrated the BICs that arise in systems due to the destructive interference of nonorthogonal eigenmodes (FW-BIC).⁷ Later, the BICs were found in acoustic^{8–11} and electrodynamic^{12,13} systems. The BICs are used to create ultrahigh-Q cavities,¹⁴ laser sources,^{15–18} sensors,^{19,20} optical vortex sources,^{21,22} and perfect absorbers.^{23,24} The Q factor of the resonance near a BIC (quasi-BIC) can be tuned by changing the energy radiative decay rate from the resonant mode by changing the parameters of the system.²⁵ Therefore, the BIC conception is very attractive for designing of different photonic devices.²⁶

In 1D systems, the BICs can be implemented by introducing anisotropic materials.^{27–31} The anisotropic materials conventionally

used in photonics are liquid crystals (LCs), which are characterized by a high anisotropy and sensitivity to external fields, allowing for dynamic tuning of the optical properties. The introduction of LC materials as a resonator layer into a 1D photonic crystal (PhC) makes it possible to tune both the position of the resonance^{32,33} as well as the width of the quasi-BIC.^{34–36}

In our previous work,³⁴ we demonstrated a tunable Q factor of a quasi-BIC in a microcavity with an LC resonator layer sandwiched between PhC and opaque gold (Au) mirrors.³⁷ The presence of the opaque Au layer made it possible to measure the reflectance spectra only from the PhC side and only with TM-polarization. In this work, we replaced the opaque Au layer by a semitransparent one, which leads to important effects. In particular, the proposed design allows for excitation of resonances from both sides, PhC and Au, and by both TE and TM polarized incident waves. This enables observing resonances in both reflectance and transmittance spectra of the system and leads to resonant polarization conversion. Although it is impossible to implement a true BIC due to the radiation loss through the

semitransparent Au layer, the Q factor can be tuned, which is demonstrated using three methods: mechanical rotation of the sample, heating, and application of external voltage.

The microcavity consists of PhC and Au mirrors deposited onto a glass substrates [see Fig. 1(a)]. The glass substrate for the PhC mirror was precoated with an indium tin oxide (ITO) conductive layer. The PhC includes eight Si₃N₄ and SiO₂ bilayers and an additional Si₃N₄ layer on top. The optical and geometric parameters of the layers and the fabrication technique are reported in Sec. I in the supplementary material. The parameters of the PhC were optimized to obtain the center of the photonic bandgap (PBG) at wavelength $\lambda = 580$ nm at Brewster's angle.

An anisotropic 4-pentyl-4'-cyanobiphenyl (5CB) nematic LC layer is sandwiched between the PhC and semitransparent Au mirrors. The gap between the PhC and the Au mirror is controlled by using Teflon spacers. Polyvinyl alcohol (PVA) layers are deposited onto the PhC and Au mirrors and unidirectionally rubbed for a planar alignment of the LC. The LC permittivity ellipsoid axis is determined by

the preferred direction of the long molecular axis. The preferred direction of the long molecular axis is defined by the unit vector $\mathbf{a} = [\cos(\phi) \cos(\theta); \sin(\phi) \cos(\theta); \sin(\theta)]$, called the director. In the LC layer, the electric field vector for the ordinary waves (*o*-waves) and extraordinary (*e*-waves) waves has the following form: $\mathbf{E}_o = E_o[\mathbf{a} \times \boldsymbol{\kappa}_o]$, $\mathbf{E}_e = E_e[\mathbf{a} - \frac{\epsilon_e(\alpha)}{\epsilon_o} \boldsymbol{\kappa}_e(\boldsymbol{\kappa}_e \mathbf{a})]$.³⁸ The propagation directions for the *o*- and *e*-waves are specified by the unit vectors $\boldsymbol{\kappa}_{o,e} = \frac{\mathbf{k}_{o,e}}{|\mathbf{k}_{o,e}|} = (\kappa_{o,ex}; 0; \kappa_{o,ez})$, where α is the angle between the vectors \mathbf{a} and $\boldsymbol{\kappa}_e$, and $\epsilon_e(\alpha)$ is the permittivity for the *e*-wave. The initial planar alignment without external voltage corresponds to the case $\theta = 0, \phi = 0$ over the entire LC layer. In general, if $\theta \neq 0$ and $\phi \neq 0$, the vectors $\mathbf{E}_{o,e}$ have all three Cartesian components, which leads to mixing of the TE polarized waves (TE-waves) with the components $[0; E_y; 0]$ and the TM polarized waves (TM-waves) with the components $[E_x; 0; E_z]$ in the LC layer.

Figures 1(b) and 1(d) show the transmittance spectra measured and calculated by Berreman's transfer matrix method³⁹ for isolated PhC and Au mirrors at the normal incidence. For the *x*- and *y*-polarized

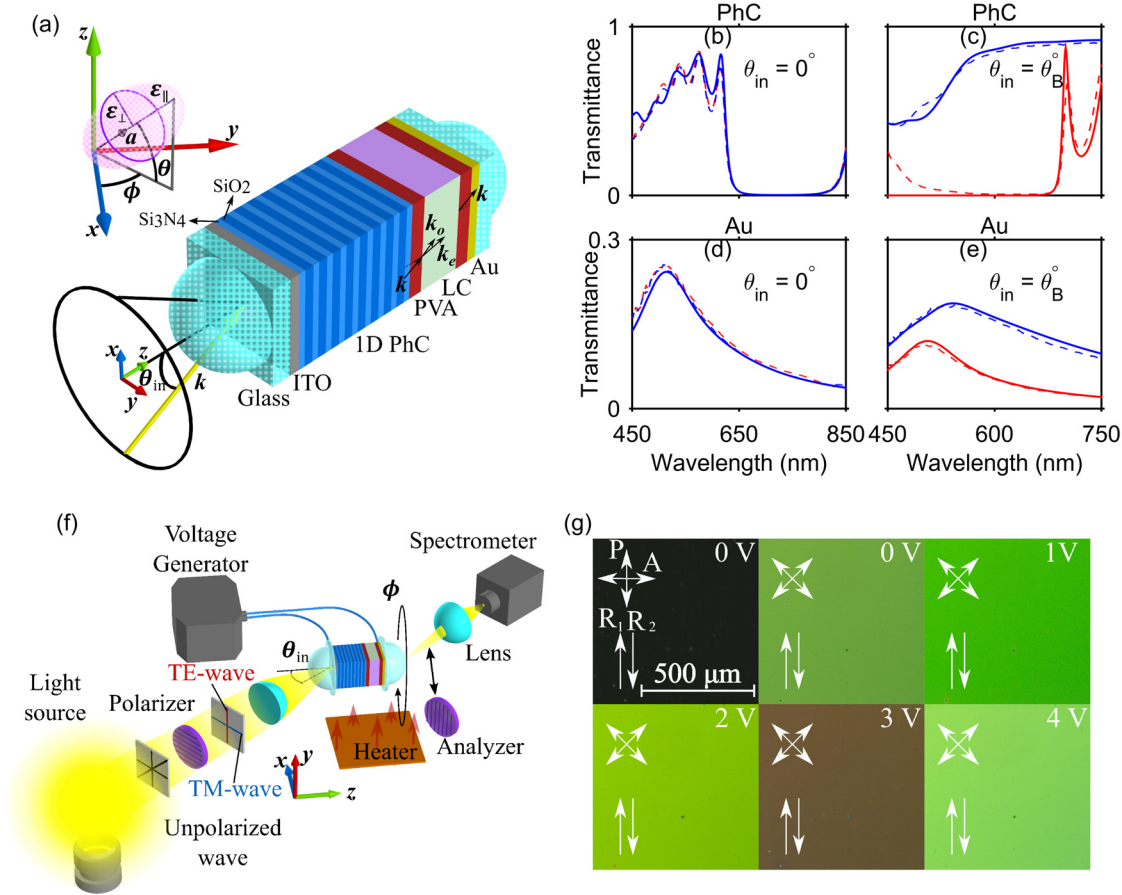


FIG. 1. (a) Model of an optical microcavity. The inset shows the LC permittivity ellipsoid orientation. (b) and (d) Experimental (dashed lines) and calculated (solid lines) transmittance spectra of the PhC and Au mirrors at the normal incidence of the *y*-polarized (red) and *x*-polarized (blue) waves. (c) and (e) Experimental (dashed lines) and calculated (solid lines) transmittance spectra of the PhC and Au mirrors at the Brewster angle for the TE (red) and TM (blue) waves. (f) Experimental scheme for measuring the transmittance spectra. (g) Polarizing optical microscopy images of the LC layer texture taken in crossed polarizers at different applied voltages. R₁ and R₂ are the PVA rubbing directions. Double arrows show the polarizer (P) and analyzer (A) directions.

28 August 2023 05:39:10

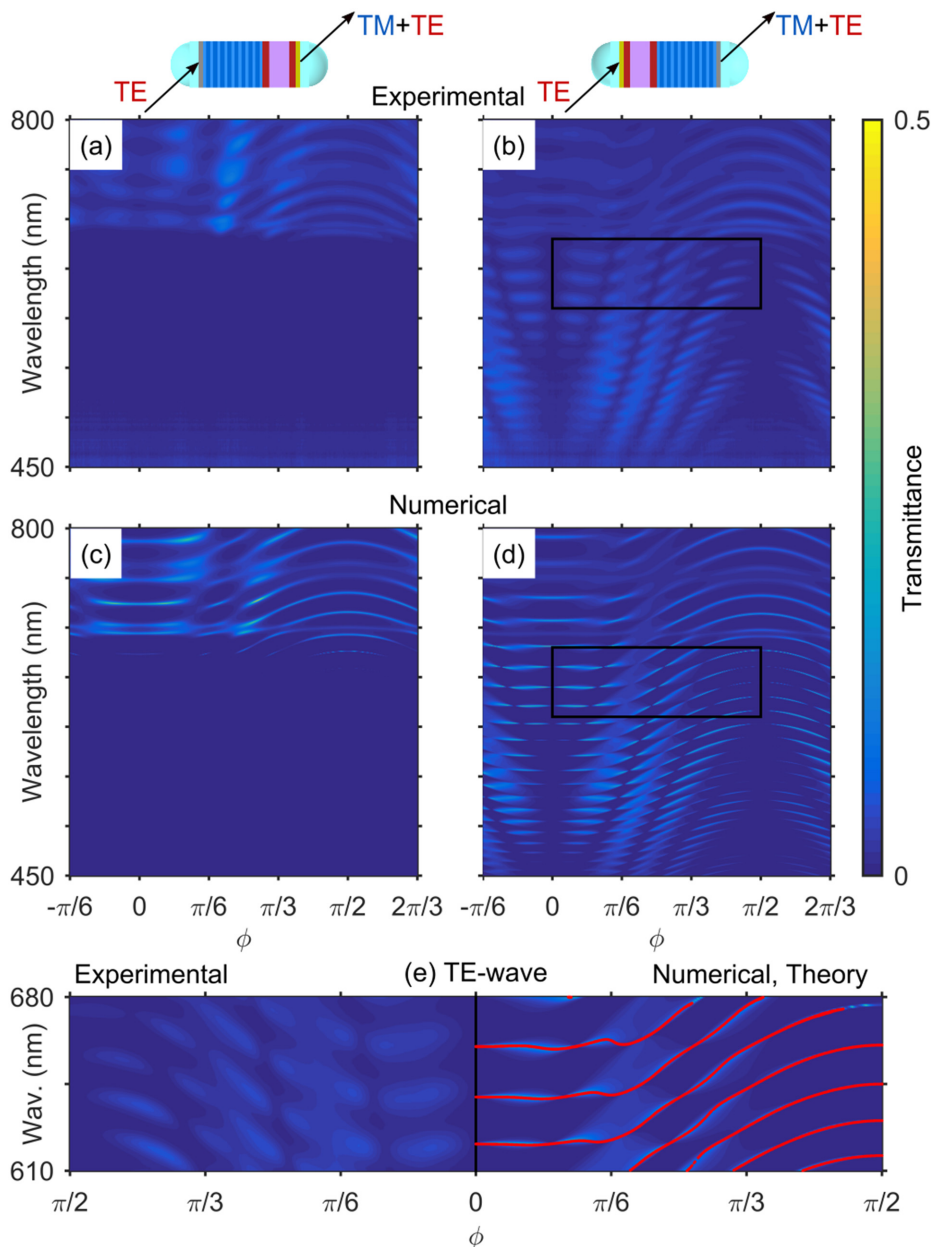


FIG. 2. Experimental [(a) and (b)] and calculated [(c) and (d)] transmittance spectra of the microcavity at different azimuthal angles ϕ of the TE-wave incidence from the PhC side ($h_{LC} = 9.2 \mu\text{m}$) [(a) and (c)] and from the Au side ($h_{LC} = 9.9 \mu\text{m}$) [(b) and (d)]. The plots in (a)–(d) share the same colorbar and the same axes. The vertical axis labels are presented on the left and the horizontal axis labels, at the bottom. The areas enclosed in black rectangles are shown zoomed in (e). Red solid lines correspond to the solution of the eigenvalue problem for the open cavity.

waves, a PBG with the center at $\lambda = 700 \text{ nm}$ is observed. The semitransparent Au mirror exhibits the maximum transmittance at $\lambda = 520 \text{ nm}$. When light is incident at Brewster's angle, the PBG for the TE-waves shifts to the short-wavelengths [see Fig. 1(c)]. At the same time, the PBG for the TM-waves vanishes due to the Brewster effect. Figure 1(e) presents the measured and calculated transmittance spectra of the TE and TM-waves for the Au mirror at the same incidence angle. It can be seen that, in contrast to the PhC mirror, the Au mirror can transmit light of both polarizations in the PBG range.

The transmittance spectra of the microcavity were measured using the experimental setup shown in Fig. 1(f), which is described in

Sec. II of the supplementary material. Figure 1(g) presents the LC optical texture images of the layer obtained in a crossed polarizer scheme of a polarizing microscope. The dark optical texture was observed when the PVA rubbing direction was parallel to one of the polarizers and the maximum light texture was observed at an angle of $\pi/4$ between the PVA rubbing direction and the polarizer. This evidences for the planar orientation in the LC layer. When a voltage is applied, the director aligns with the external electric field, i.e., the polar angle θ of the LC director \mathbf{a} increases. In this case, the $\varepsilon_e(\alpha)$ of the anisotropic layer changes, which manifests itself in a change in the color of the optical texture upon variation of the applied voltage amplitude.

At high voltages, the transition from the planar to homeotropic orientation occurs.

Figure 2 presents the experimental and calculated transmittance spectra of the microcavity at different azimuthal angles ϕ . Figures 2(a) and 2(c) correspond to the TE-wave incident from the PhC side. In the transmittance spectra, no obvious spectral manifestation of the microcavity modes in the PBG region is observed. At $\lambda > 700$ nm, there are resonant lines caused by poor reflection of the TE-waves behind the PBG red edge. When the TE-waves are incident from the Au side, there are multiple resonant lines with variable positions and widths in the PBG region [seen in Figs. 2(b) and 2(d)]. The red shift of the resonant lines is explained by the fact that, at $\phi = 0, \pi/2$, the polarizations do not mix in the LC layer. Due to the Bragg diffraction, only the TE-waves with the permittivity changing from ϵ_{\perp} to ϵ_{\parallel} are localized. In addition, multiple vanishing resonant lines are observed.

To explain the features of the spectra, we apply the temporal coupled-mode theory (TCMT). The microcavity mode can lose its energy through three radiation channels, the coupling to which is characterized by coupling constants d_1, d_2 , and d_3 . The first radiation

channel corresponds to the TM-waves in the PhC, while the second and third channels correspond to the TM- and TE-waves behind the Au layer, respectively. For the coupling constants, we have $d_{1,2} \propto \sqrt{\gamma_{TM}}$ and $d_3 \propto \sqrt{\gamma_{TE}}$, where γ_{TM} and γ_{TE} are the radiative decay rates into the continuum of TM- and TE-waves, respectively. Under variation in the azimuthal angle ϕ , the decay rate γ_{TM} changes, which manifests itself as a change in the resonant linewidth. The decay rate γ_{TM} is proportional to the Poynting vector of the TM component of the resonant mode at the LC layer boundary: $\gamma_{TM} \propto |E_x|^2$. There are two possibilities with $\gamma_{TM} = 0$. The first corresponds to the planar LC orientation at which the TE and TM polarizations do not mix, $\phi = 0$ or $\pi/2, \theta = 0$. In the second case, the LC mixes the TE and TM polarizations and a mode with both components is localized in the cavity layer. Since the $\epsilon_e(\alpha)$ value depends on ϕ , then the phase difference between the o - and e -waves at the LC layer output depends on the angle ϕ . At certain ϕ values, the o - and e -waves at the LC layer output cancel out to yield a zero outgoing TM-wave component $E_x = E_{ox} + E_{ex} = 0$. These two possibilities are discussed in detail in Sec. III of the supplementary material.

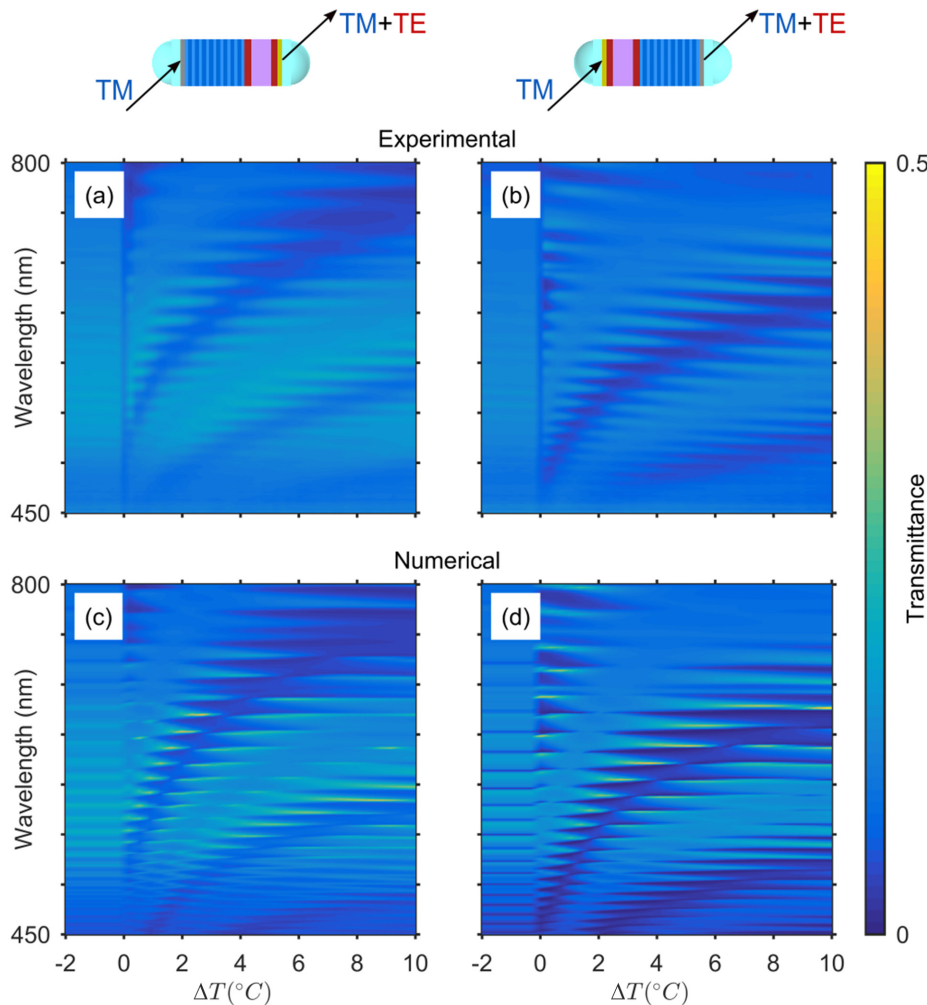


FIG. 3. Experimental [(a) and (b)] and calculated [(c) and (d)] transmittance spectra of the microcavity at the TM-wave incident from the PhC side ($h_{LC} = 10.2 \mu\text{m}$) [(a) and (c)] and from the Au side ($h_{LC} = 8.8 \mu\text{m}$) [(b) and (d)] under variation in the LC layer temperature, $\Delta T = T_c - T$, where $T_c = 35.2$ C is the temperature of the 5CB LC phase transition to the isotropic phase.

The PhC mirror in the PBG region transmits only TM-waves acting as a polarizer. According to the transmittance spectra in Figs. 2(b) and 2(d), the resonant conversion of the incident TE-waves into the transmitted TM-waves occurs. Within the TCMT, the resonant transmittance from the TE to TM-waves is given by

$$S_{13} = C_{13} + \frac{d_1 d_3}{i(\omega_0 - \omega) + \gamma}, \quad (1)$$

where $\gamma = \gamma_{\text{TM}} + \gamma_{\text{TE}} + \gamma_0$. The derivation of Eq. (1) is presented in Sec. V of the supplementary material. When the first channel is closed, $d_1 = 0$, the resonant line vanishes with a finite width, since the radiative decay rate γ_{TE} and the material loss rate γ_0 are always nonzero. This is confirmed by solving the eigenfrequency problem for the open cavity. The eigenfrequency is a complex number $\omega_r = \omega_0 - i\gamma$. The equations for ω_r are derived by wave matching with the radiation boundary conditions.³⁴ The spectral positions of the resonant lines determined by the real part of the eigenfrequency ω_0 agree well with the obtained spectra [see Fig. 2(e)]. Figure S1 in the supplementary material shows the angular dependence of the imaginary part of the eigenfrequency γ near $\phi = 0$ for two cases, namely, with and without an account of absorption in the Au layer. The calculations show that, even in the absence of absorption, we have $\gamma(\phi = 0) \equiv \gamma_{\text{TE}} \neq 0$, which indicates radiation loss into the TE channel. Therefore, a true BIC did not occur in the system despite the typical spectral

manifestation in the form of vanishing resonant lines.⁴⁰ In this case, it is still possible to control the Q factor of the microcavity by changing the radiation decay rate to the TM channel.

Due to the sensitivity of the liquid crystal to the external factors, we can use two different approaches for tuning the resonant line position and width, thermal and electric. The temperature tuning of the spectra was achieved by heating the planar oriented LC layer with $\theta = 0$. Figure 3 presents the experimental and calculated transmittance spectra for the TM-wave incident from the PhC and Au sides with the LC director oriented at an angle of $\phi = \pi/4$. Below the temperature $T_c = 35.2^\circ\text{C}$ of the phase transition of the LC to the isotropic phase, multiple resonant lines are observed. As the temperature increases, the resonant line shift turns out to be insignificant since, at $\phi = \pi/4$, the decrease in ϵ_{\parallel} is compensated by the increase in ϵ_{\perp} ⁴¹ [see Sec. VI of the supplementary material]. The permittivities of the LC layer change upon heating and, at certain temperatures, the resonant lines vanish, as explained above. At $T > T_c$, the anisotropic LC transforms to the isotropic state, in which the polarizations do not mix, i.e., the TE-wave amplitude is zero over the entire LC volume. The small-amplitude and constant-width resonances are due to the weak reflection of the TM-waves at the Au/PVA and PVA/Si₃N₄ interfaces.

Figure 4 illustrates the transformation of the microcavity transmittance spectra, when an 1 kHz external voltage is applied to the

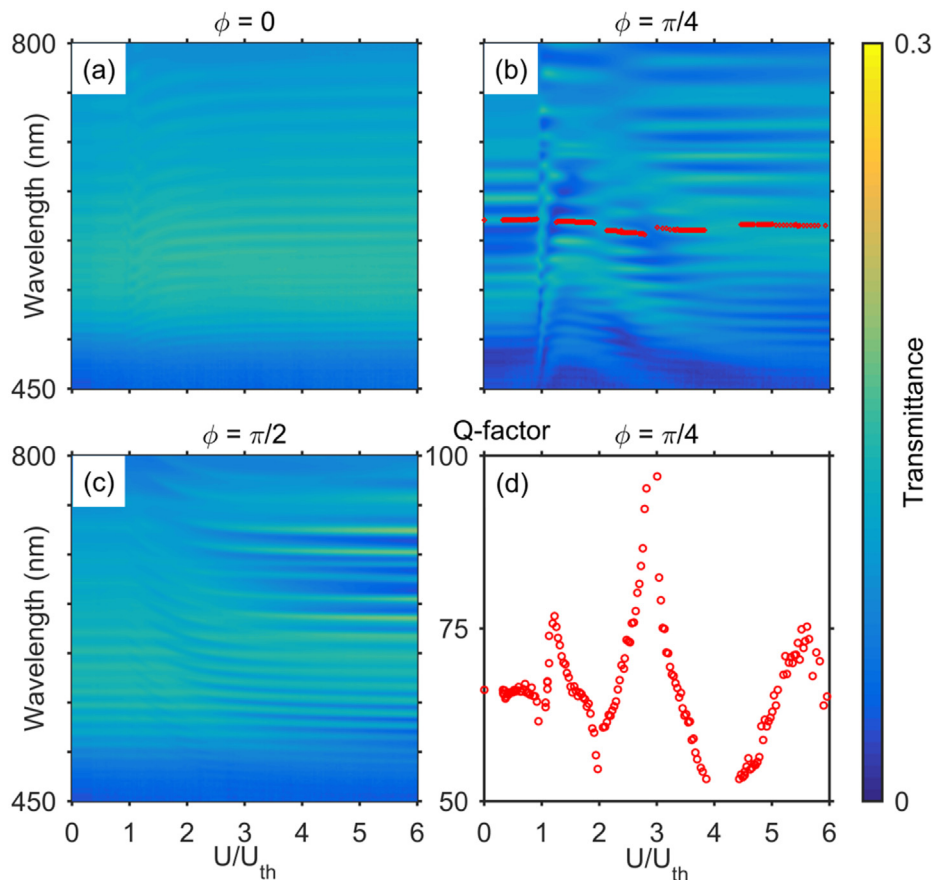


FIG. 4. Measured transmittance spectra for the incident TM-waves at different applied voltages and a fixed azimuthal angle of the LC director rotation, (a) $\phi = 0$, (b) $\pi/4$, and (c) $\pi/2$. The threshold voltage is $U_{\text{th}} \approx 0.9$ V. (d) Q factor of the resonant line [red circles in Fig. 4(b)] calculated from the full width at half maximum.

conductive Au and ITO layers. The transmittance spectra at azimuthal angles of $\phi = 0, \pi/4, \pi/2$ for a TM-wave incident from the Au side were measured. Under voltages below U_{th} , the position and width of the resonances remain constant due to the invariance of the LC structure alignment. At $U > U_{th}$, LC molecules rearrange due to the Frederiks effect. The director tends to orient along the applied field in the z -axis direction, which leads to an increase in the polar angle θ . The $\varepsilon_e(\alpha)$ changes, which causes a change in the position and width of the resonant lines. At $\phi = 0$, for all polar angles θ , the polarizations in the LC layer do not mix. It means that the coupling with the first radiation channel is canceled, $d_1 = 0$. In the spectrum presented in Fig. 4(a), the small-amplitude constant-width resonances are observed, which correspond, as explained above, to the weak TM-wave localization. At $\phi = \pi/4, \pi/2$, and $\theta \neq 0$ the polarizations in the LC layer are mixed, as shown Figs. 4(b) and 4(c). At certain U values, the resonant lines vanish, $d_1 = 0$. In the limiting case, at high voltages U , the LC molecules are oriented along the z axis and the LC permittivity for resonant electromagnetic waves takes the minimum possible value ε_{\perp} , which results in a blue shift of the resonant lines [see Sec. VII of the supplementary material]. Figure 4(d) illustrates the change in the Q factor of the resonant line highlighted with red circles in Fig. 4(b). At the vanishing point, the resonance Q factor is doubled with a change in the external voltage by only 1 V. The maximum value of the measured Q-factor is ~ 100 for voltage application experiment [see Fig. 4(d)] and ~ 130 for mechanical rotation of the sample [Fig. S4(a)]. This value is approximately twice larger in comparison with previous results for a nontransparent Au layer where the maximum value of the Q-factor was $\sim 40\text{--}70$.^{34,35}

In this work, an optical microcavity consisting of a nematic liquid crystal layer, a semitransparent gold mirror, and a photonic crystal operating at Brewster's angle is proposed. A number of important effects were experimentally demonstrated and theoretically explained, namely, (i) excitation of the resonant modes by both the TE and TM polarizations from both the photonic crystal and gold mirror sides; (ii) the resonant transmission between the channels of different polarizations; and (iii) a tunable Q factor by mechanical rotation, heating of the sample, and applying an external voltage to the liquid crystal layer. The results obtained can be used to create energy-efficient photonics devices, including dye microlasers,³³ perfect light absorbers,³⁵ and sensors.²⁰

See the supplementary material for information about parameters of the microcavity, experimental setup, explanation of vanishing of resonances, resonant transmission, temporal coupled-mode theory, temperature tunability, and voltage tunability.

The authors are grateful to Alexander S. Krylov (Kirensky Institute of Physics SB RAS) for helpful discussions. This work was supported by the Russian Science Foundation under Grant No. 22-42-08003. This research was also funded by the National Science and Technology Council (NSTC 111-2923-E-007-008-MY3 and 111-2628-E-007-021). The authors would like to express their special gratitude to the Krasnoyarsk Regional Center for Collective Use of the Federal Research Center "Krasnoyarsk Scientific Center, Siberian Branch of the Russian Academy of Sciences" for providing equipment within this project.

AUTHOR DECLARATIONS

Conflict of Interest

The authors have no conflicts to disclose.

Author Contributions

Gavriil A. Romanenko: Data curation (equal); Investigation (lead); Software (equal); Validation (equal); Visualization (lead); Writing – original draft (lead); Writing – review & editing (equal). **Nikita A. Zolotovskiy:** Investigation (equal); Writing – review & editing (equal). **Igor A. Tambasov:** Investigation (equal); Writing – review & editing (equal). **Michail N. Volochev:** Investigation (equal); Writing – review & editing (equal). **Kuo-Ping Chen:** Investigation (equal); Supervision (equal); Writing – review & editing (equal). **Ivan V. Timofeev:** Investigation (equal); Supervision (equal); Writing – review & editing (equal). **Pavel S. Pankin:** Conceptualization (equal); Funding acquisition (equal); Methodology (equal); Supervision (equal); Writing – original draft (equal); Writing – review & editing (equal). **Daniil S. Buzin:** Investigation (equal); Software (equal). **Dmitrii N. Maksimov:** Investigation (equal); Writing – review & editing (equal). **Vitaly S. Sutormin:** Investigation (equal); Writing – review & editing (equal). **Aleksey I. Krasnov:** Investigation (equal); Writing – review & editing (equal). **Fyodor V. Zelenov:** Investigation (equal); Writing – review & editing (equal). **Albert N. Masyugin:** Investigation (equal); Writing – review & editing (equal). **Sergey V. Nedelin:** Investigation (equal); Writing – review & editing (equal).

DATA AVAILABILITY

The data that support the findings of this study are available from the corresponding author upon reasonable request.

REFERENCES

- A. F. Sadreev, "Interference traps waves in an open system: Bound states in the continuum," *Rep. Prog. Phys.* **84**, 055901 (2021).
- J. von Neumann and E. P. Wigner, "Über merkwürdige diskrete Eigenwerte," *Z. Phys.* **30**, 465–467 (1929).
- F. H. Stillinger and D. R. Herrick, "Bound states in the continuum," *Phys. Rev. A* **11**, 446–454 (1975).
- D. R. Herrick, "Construction of bound states in the continuum for epitaxial heterostructure superlattices," *Physica B + C* **85**, 44–50 (1976).
- M. Robnik, "A simple separable Hamiltonian having bound states in the continuum," *J. Phys. A* **19**, 3845–3848 (1986).
- K. L. Koshelev, Z. F. Sadrieva, A. A. Shcherbakov, Y. S. Kivshar, and A. Bogdanov, "Bound states in the continuum in photonic structures," *Phys.-Usp.* **65**, 494–517 (2022).
- H. Friedrich and D. Wintgen, "Interfering resonances and bound states in the continuum," *Phys. Rev. A* **32**, 3231–3242 (1985).
- A. A. Lyapina, D. N. Maksimov, A. S. Pilipchuk, and A. F. Sadreev, "Bound states in the continuum in open acoustic resonators," *J. Fluid Mech.* **780**, 370–387 (2015).
- Z. Yu and X. Sun, "Acousto-optic modulation of photonic bound state in the continuum," *Light Sci. Appl.* **9**, 1–9 (2020).
- S. Huang, S. Xie, H. Gao, T. Hao, S. Zhang, T. Liu, Y. Li, and J. Zhu, "Acoustic Purcell effect induced by quasibound state in the continuum," *Fundam. Res.* (published online, 2022).
- M. S. Sidorenko, O. N. Sergaeva, Z. F. Sadrieva, C. Roques-Carmes, P. S. Muraev, D. N. Maksimov, and A. A. Bogdanov, "Observation of an accidental bound state in the continuum in a chain of dielectric disks," *Phys. Rev. Appl.* **15**, 034041 (2021).
- A. F. Sadreev, E. N. Bulgakov, and I. Rotter, "Bound states in the continuum in open quantum billiards with a variable shape," *Phys. Rev. B* **73**, 235342 (2006).

- ¹³E. N. Bulgakov and A. F. Sadreev, "Bound states in the continuum in photonic waveguides inspired by defects," *Phys. Rev. B* **78**, 075105 (2008).
- ¹⁴M. V. Rybin, K. L. Koshelev, Z. F. Sadrieva, K. B. Samusev, A. A. Bogdanov, M. F. Limonov, and Y. S. Kivshar, "High-q supercavity modes in subwavelength dielectric resonators," *Phys. Rev. Lett.* **119**, 243901 (2017).
- ¹⁵A. Kodigala, T. Lepetit, Q. Gu, B. Bahari, Y. Fainman, and B. Kanté, "Lasing action from photonic bound states in continuum," *Nature* **541**, 196–199 (2017).
- ¹⁶S. T. Ha, Y. H. Fu, N. K. Emani, Z. Pan, R. M. Bakker, R. Paniagua-Domínguez, and A. I. Kuznetsov, "Directional lasing in resonant semiconductor nanoantenna arrays," *Nat. Nanotechnol.* **13**, 1042–1047 (2018).
- ¹⁷M. Wu, S. T. Ha, S. Shendre, E. G. Durmusoglu, W.-K. Koh, D. R. Abujetas, J. A. Sánchez-Gil, R. Paniagua-Domínguez, H. V. Demir, and A. I. Kuznetsov, "Room-temperature lasing in colloidal nanoplatelets via Mie-resonant bound states in the continuum," *Nano Lett.* **20**, 6005–6011 (2020).
- ¹⁸J.-H. Yang, Z.-T. Huang, D. N. Maksimov, P. S. Pankin, I. V. Timofeev, K.-B. Hong, H. Li, J.-W. Chen, C.-Y. Hsu, Y.-Y. Liu *et al.*, "Low-threshold bound state in the continuum lasers in hybrid lattice resonance metasurfaces," *Laser Photonics Rev.* **15**, 2100118 (2021).
- ¹⁹S. Romano, M. Mangini, E. Penzo, S. Cabrini, A. C. De Luca, I. Rendina, V. Mocella, and G. Zito, "Ultrasensitive surface refractive index imaging based on quasi-bound states in the continuum," *ACS Nano* **14**, 15417–15427 (2020).
- ²⁰Z. A. Zaky, B. Moustafa, and A. H. Aly, "Plasma cell sensor using photonic crystal cavity," *Opt. Quantum Electron.* **53**, 1–13 (2021).
- ²¹H. M. Doleman, F. Monticone, W. den Hollander, A. Alù, and A. F. Koenderink, "Experimental observation of a polarization vortex at an optical bound state in the continuum," *Nat. Photonics* **12**, 397–401 (2018).
- ²²L. Kang, Y. Wu, X. Ma, S. Lan, and D. H. Werner, "High-harmonic optical vortex generation from photonic bound states in the continuum," *Adv. Opt. Mater.* **10**, 2101497 (2022).
- ²³Z. Wang, Y. Liang, J. Qu, M. K. Chen, M. Cui, Z. Cheng, J. Zhang, J. Yao, S. Chen, D. P. Tsai *et al.*, "Plasmonic bound states in the continuum for unpolarized weak spatially coherent light," *Photonics Res.* **11**, 260–269 (2023).
- ²⁴R. G. Bikbaev, D. N. Maksimov, P. S. Pankin, M.-J. Ye, K.-P. Chen, and I. V. Timofeev, "Enhanced light absorption in tamm metasurface with a bound state in the continuum," [arXiv:2301.04346](https://arxiv.org/abs/2301.04346) (2023).
- ²⁵C. Zhou, L. Huang, R. Jin, L. Xu, G. Li, M. Rahmani, X. Chen, W. Lu, and A. E. Miroshnichenko, "Bound states in the continuum in asymmetric dielectric metasurfaces," *Laser Photonics Rev.* **17**, 2200564 (2023).
- ²⁶S. I. Azzam and A. V. Kildishev, "Photonic bound states in the continuum: From basics to applications," *Adv. Opt. Mater.* **9**, 2001469 (2021).
- ²⁷J. Gomis-Bresco, D. Artigas, and L. Torner, "Anisotropy-induced photonic bound states in the continuum," *Nat. Photonics* **11**, 232–236 (2017).
- ²⁸I. V. Timofeev, D. N. Maksimov, and A. F. Sadreev, "Optical defect mode with tunable q factor in a one-dimensional anisotropic photonic crystal," *Phys. Rev. B* **97**, 024306 (2018).
- ²⁹P. S. Pankin, D. N. Maksimov, and I. V. Timofeev, "Bound state in the continuum in an anisotropic photonic crystal supported by a full-wave phase plate," *JOSA B* **39**, 968–972 (2022).
- ³⁰P. S. Pankin, D. N. Maksimov, K.-P. Chen, and I. V. Timofeev, "Fano feature induced by a bound state in the continuum via resonant state expansion," *Sci. Rep.* **10**, 13691 (2020).
- ³¹S. V. Nabol, P. S. Pankin, D. N. Maksimov, and I. V. Timofeev, "Fabry-Perot bound states in the continuum in an anisotropic photonic crystal," *Phys. Rev. B* **106**, 245403 (2022).
- ³²R. Ozaki, T. Matsui, M. Ozaki, and K. Yoshino, "Electro-tunable defect mode in one-dimensional periodic structure containing nematic liquid crystal as a defect layer," *Jpn. J. Appl. Phys., Part 2* **41**, L1482 (2002).
- ³³R. Ozaki, T. Matsui, M. Ozaki, and K. Yoshino, "Electrically color-tunable defect mode lasing in one-dimensional photonic-band-gap system containing liquid crystal," *Appl. Phys. Lett.* **82**, 3593–3595 (2003).
- ³⁴P. S. Pankin, B.-R. Wu, J.-H. Yang, K.-P. Chen, I. V. Timofeev, and A. F. Sadreev, "One-dimensional photonic bound states in the continuum," *Commun. Phys.* **3**, 1–8 (2020).
- ³⁵B.-R. Wu, J.-H. Yang, P. S. Pankin, C.-H. Huang, W. Lee, D. N. Maksimov, I. V. Timofeev, and K.-P. Chen, "Quasi-bound states in the continuum with temperature-tunable Q factors and critical coupling point at Brewster's angle," *Laser Photonics Rev.* **15**, 2000290 (2021).
- ³⁶A. Krasnov, P. Pankin, D. Buzin, G. Romanenko, V. Sutormin, F. Zelenov, A. Masyugin, M. Volochaev, S. Y. Vetrov, and I. Timofeev, "Voltage-tunable Q factor in a photonic crystal microcavity," *Opt. Lett.* **48**, 1666–1669 (2023).
- ³⁷M. Kaliteevski, I. Iorsh, S. Brand, R. Abram, J. Chamberlain, A. Kavokin, and I. Shelykh, "Tamm plasmon-polaritons: Possible electromagnetic states at the interface of a metal and a dielectric Bragg mirror," *Phys. Rev. B* **76**, 165415 (2007).
- ³⁸F. V. Ignatovich and V. K. Ignatovich, "Optics of anisotropic media," *Phys.-Usp.* **55**, 709 (2012).
- ³⁹D. W. Berreman, "Optics in stratified and anisotropic media: 4 × 4-matrix formulation," *JOSA* **62**, 502–510 (1972).
- ⁴⁰C. W. Hsu, B. Zhen, J. Lee, S.-L. Chua, S. G. Johnson, J. D. Joannopoulos, and M. Solja, "Observation of trapped light within the radiation continuum," *Nature* **499**, 188–191 (2013).
- ⁴¹S.-T. Wu, C. Wu, M. Warengem, and M. Ismaili, "Refractive index dispersions of liquid crystals," *Opt. Eng.* **32**, 1775–1780 (1993).